Adsorption (2007) 13: 501–508
DOI 10.1007/s10450-007-9022-8

Quantum effect induced kinetic molecular sieving of hydrogen and deuterium in microporous materials

A.V. Anil Kumar · Hervé Jobic · Suresh K. Bhatia

Received: 18 April 2007 / Revised: 5 July 2007 / Accepted: 11 July 2007 / Published online: 13 September 2007

Abstract We report here our investigations using Monte Carlo and molecular dynamics (MD) simulations, as well as quasi-elastic neutron scattering experiments, to study the adsorption and diffusion of H_2 and D_2 in zeolite Rho. In the simulations, quantum effects are incorporated via the Feynman-Hibbs variational approach. At low temperatures, we observe a reversal of kinetic molecular sieving in which D_2 diffuses faster than H_2. Based on fits of bulk data, we suggest new set of potential parameters for hydrogen, with the Feynman-Hibbs variational approach used for quantum corrections. The transport properties obtained from MD simulations are in excellent agreement with the experimental results, with both showing significant quantum effects on the transport at low temperature. The MD simulation results on two different structures of zeolite Rho clearly demonstrate that the quantum effect is very sensitive to pore size. High transport flux selectivity is noted at low temperatures, suggesting feasibility of kinetic isotope separation.

Keywords Quantum effect · Kinetic molecular sieving · Isotope separation · Hydrogen adsorption · Molecular dynamics

A.V. Anil Kumar · S.K. Bhatia (✉)
Department of Chemical Engineering, The University of Queensland, Brisbane, QLD-4072, Australia
e-mail: s.bhatia@eng.uq.edu.au

H. Jobic
IRCELYON, Institut de Recherches sur la Catalyse et l'Environnement de LYON, CNRS, Université de Lyon, UMR5256, 2 Avenue A. Einstein, 69626 Villeurbanne, France

1 Introduction

Guest-host systems consisting of molecules confined in microstructured porous materials have found wide spread applications in mixture separations, catalysis and ion exchange (Karger and Ruthven 1992; Yang 2003). Crystalline microporous materials use their size and shape selectivity to separate the components from their mixture. However, they are seldom used for separating isotope mixtures. This is because, from the classical viewpoint, different isotopes are identical in size and shape. Alternative expensive and tedious processes like centrifugation, laser isotope separation and thermal distillation, are therefore used to separate isotope mixtures, particularly those of hydrogen isotopes. It will be of great advantage, if one would be able to use microporous materials for the separation of hydrogen isotopes, as an alternative to the conventional methods.

When the pore dimensions in the microporous materials are narrow enough, the hydrogen molecule and its isotopes can no longer be considered as classical particles, as is common. At pore dimensions of the order of de Broglie wavelength and low enough temperatures, quantum effects are significant and can no longer be neglected. Quantum considerations in the study of equilibrium adsorption of hydrogen isotopes in micro porous materials have already demonstrated that heavier isotopes are adsorbed more strongly than lighter ones. This was first proposed by Beenaker et al., while studying the adsorption of hard sphere molecules in hard cylinders (Beenaker et al. 1995), and later verified by Sholl and coworkers using analytical and path integral Monte Carlo simulations (Wang et al. 1999; Challa et al. 2001). However, all these studies have been confined to equilibrium adsorption and the importance of quantum effects on the dynamics is poorly understood. Recently, we (Kumar and Bhatia 2005) have investigated the

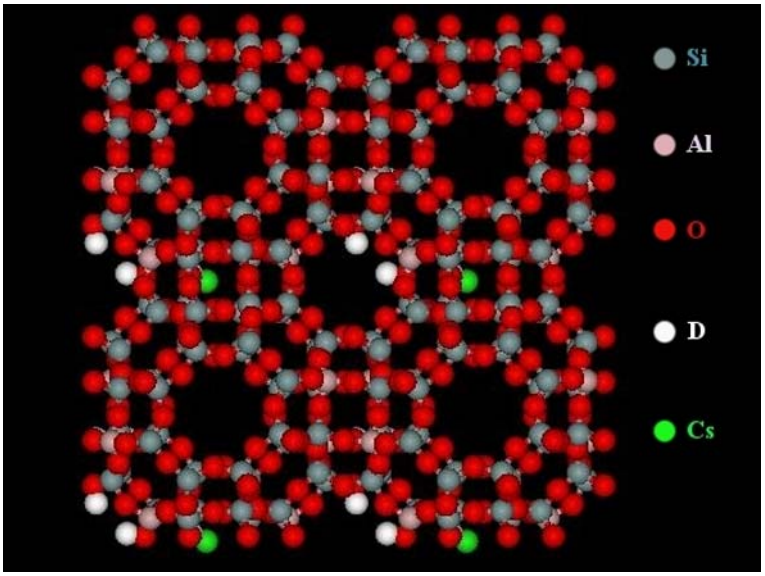

Fig. 1 $2 \times 2 \times 2$ Unit cells of zeolite Rho II structure. The atomic coordinates are taken from Fisher et al. (1988)

dynamics of hydrogen isotopes in micro porous materials using molecular dynamics simulations, with quantum effects incorporated via the Feynman and Hibbs (1965) formalism. The dynamics is equally sensitive to quantum effects, and exhibits subtler phenomena. At sufficiently low temperatures, there exists a quantum mediated reversal in kinetic selectivity, in which the heavier deuterium diffuses faster than lighter hydrogen. In this paper we report the investigations of this effect, using molecular dynamics simulations and quasi elastic neutron scattering (QENS) experiments with zeolite Rho as the microporous host material.

2 Feynmann-Hibbs formalism

From the path integral quantum partition function for canonical ensemble of molecules, one can obtain the Feynman-Hibbs potential as (Feynman and Hibbs 1965):

$$U_{FH}(r) = \left(\frac{6\mu}{\pi\beta\hbar^2}\right)^{3/2} \times \int dR U(|r+R|) \exp\left(-\frac{6\mu}{\beta\hbar^2}R^2\right) \quad (1)$$

where μ is the reduced mass, $\beta = 1/k_B T$, k_B is the Boltzmann constant and $\hbar$ is the Plank's constant. For small values of the de Broglie wavelength, (1) may be approximated as (Kumar and Bhatia 2005; Kumar et al. 2006)

$$U_{FH}(r) = U(r) + \frac{\beta\hbar^2}{24\mu}\left[U''(r) + \frac{2U'(r)}{r}\right] + \frac{\beta^2\hbar^4}{1152\mu^2} \times \left[\frac{15U'(r)}{r^3} + \frac{4U'''(r)}{r} + U''''(r)\right]. \quad (2)$$

An expansion including only quadratic terms has been used for the studies on bulk fluids, but is not sufficiently accurate for confined fluids. The improved approximation to the FH potential in (2) can be readily incorporated in a molecular dynamics scheme.

3 Structure of zeolite Rho

As mentioned earlier, we have used zeolite Rho as the host material in this investigation, prompted by its narrow window diameter of about 0.3 nm. We have studied two different zeolite Rho materials having different unit cell compositions: one with a unit cell composition of $Cs_{1.35}(SiAl)_{48}O_{96}D$, (hereafter denoted as Rho I) in which the Si/Al ratio is taken to be unity as these atoms were indistinguishable in diffraction experiments (Parise et al. 1984), and second with a unit cell composition of $D_{5.3}Cs_{0.7}Al_6Si_{42}O_{96}$ (denoted as Rho II) with a Si/Al ratio of 7 (Fisher et al. 1988). There are two important differences between these two structures: (i) the unit cell dimension changes from 1.4601 nm to 1.488 nm and (ii) the center-to-center window diameter changes from 0.543 nm to 0.596 nm. As we will see later, these changes, particularly the change in window dimension, play a significant role in quantum mediated reversal of kinetic selectivity. The crystalline structure of Rho II is shown in Fig. 1. The basic framework of Rho I is similar, with the differences noted above.

4 Molecular simulation details

Grand Canonical Monte Carlo (GCMC) as well as equilibrium molecular dynamics (EMD) simulations were per-

formed to model the equilibrium adsorption and dynamics of hydrogen isotopes in zeolite Rho. Following the conventional procedure, the interactions between the Si and Al atoms of the solid framework and the fluid atoms were neglected. We modeled H_2 and D_2 molecules as Lennard-Jones spheres with Feynmann-Hibbs quantum corrections. We used two different sets of potential parameters for the fluid-fluid and fluid-solid interactions. The first was taken from the literature (Buch 1994; Kiselev and Du 1981), and the second was obtained by fitting GCMC simulations to experimental bulk PVT data. Our GCMC simulation procedure follows the classical Metropolis procedure, with the probabilities of creation and deletion moves equal, so as to ensure microscopic reversibility.

Molecular dynamics simulations were carried out using a fifth order Gear predictor-corrector algorithm, and maintaining the temperature at the desired value using a Gaussian Thermostat (Evans and Morris 1990). Each simulation run comprised of 20 ns, of which the initial 5 ns trajectory was ignored in calculating average properties. The self and transport diffusivities were calculated from the single particle and center of mass mean squared displacement respectively using the Einstein equation (Allen and Tildesley 1987)

$$D = \lim_{t\to\infty} \frac{\langle |\Delta r|^2(t)\rangle}{6t}. \tag{3}$$

The 15 ns trajectory used for calculating transport properties was split into five smaller runs to estimate the error involved in the calculations.

5 Experimental details

5.1 Adsorption isotherm

The hydrogen adsorption isotherm at 77 K was measured by volumetry on a home-made instrument. The gas pressure was recorded with a MKS Baratron capacitive sensor. The zeolite Rho was activated in a glass cell on a vacuum line by slow heating up to 643 K, and the cell was then connected to the volumetric apparatus. To measure the isotherm at 80 K, the adsorption cell was plunged into liquid nitrogen, whose level was kept constant during the experiment. In these experiments the Rho II zeolite was used, as this was the only variety available (from DuPont Corporation).

5.2 Quasi-elastic neutron scattering

Quasi-elastic neutron scattering (QENS) experiments were performed on the spectrometer IN6, at the Institut Laue-Langevin, Grenoble, France. The incident neutron energy was taken as 3.12 meV, corresponding to a wavelength of 5.1 Å. Spectra were recorded at various scattering angles, corresponding to wavevector transfers, Q, ranging from 0.28 to 1.53 $Å^{-1}$. Spectra from different detectors were grouped in order to obtain reasonable counting statistics and to avoid the Bragg peaks of the zeolite. The line shape of the elastic energy resolution could be fitted by a Gaussian function, whose full width at half maximum (FWHM) varied from 82 μeV at small Q to 105 μeV at large Q.

Since the hydrogen atom has the largest neutron cross-section, the degassed zeolite Rho was exposed twice to D_2O vapor at about 470 K, in order to exchange the protons from the zeolite with deuterium atoms. The sample was then dehydrated by pumping under slow heating up to 643 K (final pressure better than 10^{-3} Pa). The zeolite was transferred inside a glovebox into a slab-shaped aluminium container, which could be connected to a gas inlet system allowing in situ adsorption. After recording the scattering of the dehydrated zeolite, transport of H_2 and D_2 at a loading of 1.4 molecules per cage was studied at various temperatures. The loadings were determined from the equilibrium pressures and from the measured adsorption isotherm.

H_2 is essentially an incoherent scatterer, allowing determination of the self-diffusivity. D_2 is both incoherent and coherent, so that in principle both the self- and transport diffusion coefficients can be determined (Jobic et al. 1999), but at low loading these two diffusivities should be similar in value.

6 Results and discussion

6.1 Molecular dynamics simulations of H_2 isotopes in Rho I using reported parameters

In these initial simulations, we used the Buch parameters to model the H_2-H_2 interactions (Buch 1994). These parameters were obtained by fitting the experimental gas-phase isotherms of hydrogen and deuterium in the temperature range −175 to 150 °C. The fluid-solid interactions are taken from literature (Kiselev and Du 1981). These interaction parameters are given in Table 1.

The transport diffusivities of H_2 and D_2 obtained from molecular dynamics simulations at various temperatures are plotted in Fig. 2. We have also calculated classical values of transport diffusivities by switching off the quantum corrections to the potential in the simulations. These values are also plotted in Fig. 2 for comparison. These results are strikingly different from those of bulk fluids reported in the literature. The self diffusivity of water is found to increase when

Table 1 Buch parameters (Buch 1994) for fluid-fluid interactions and Kiselev-Du parameters (Kiselev and Du 1981) for solid-fluid interactions

	σ (nm)	ε/k_B (K)
H_2-H_2	0.292 nm	38.0
O-H_2	0.273 nm	76.76

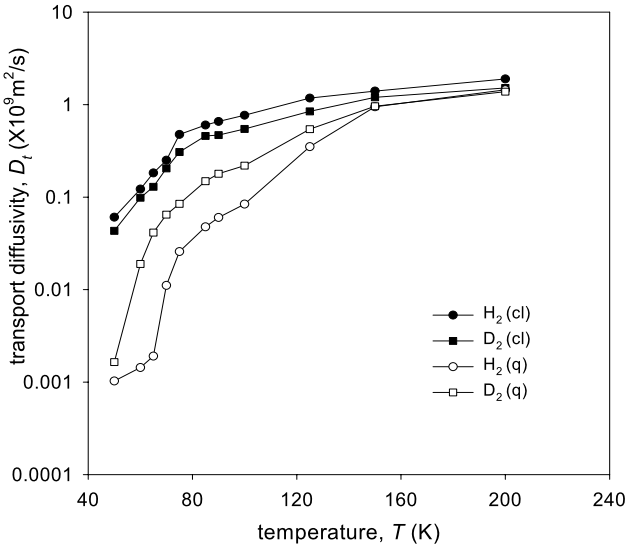

Fig. 2 Transport diffusivity of H_2 (*circle*) and D_2 (*square*) in zeolite Rho I using classical (*cl*) LJ potential (*solid symbols*) and quantum (*q*) FH potential (*open symbols*). The *points* are from molecular dynamics simulations. The *lines* are guides to the eye

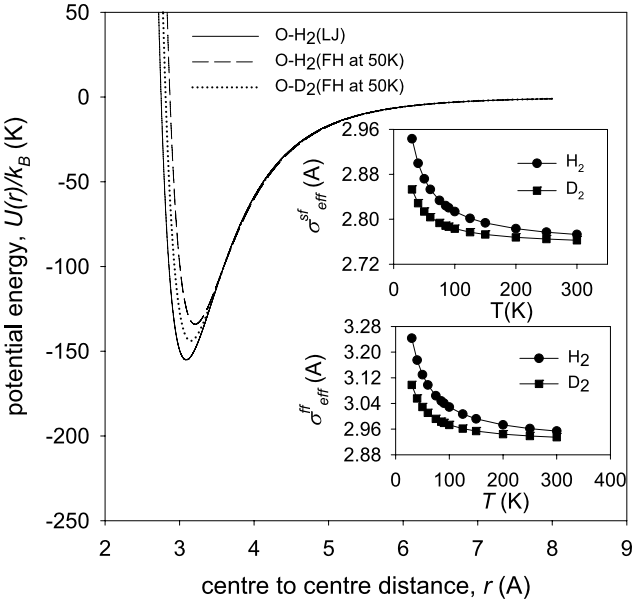

Fig. 3 The classical LJ potential (*solid line*) and the modified FH potential for H_2 (*dashed line*) and D_2 (*dotted line*) at 50 K. The temperature variations of the effective size parameters for the solid-fluid (σ_{sf}) and fluid-fluid (σ_{ff}) interactions are shown in the *insets*

quantum corrections are included in MD simulations (Guillot and Guissani 1998). To the contrary, these corrections decrease the diffusivity in the case of confined fluids, as evident from Fig. 2. More over this reduction in transport diffusivity becomes increasingly significant as the temperature is reduced. In bulk fluids, the increase in diffusivity due to quantum effects is attributed to quantum tunneling, whereby a decrease of intermolecular potential well depth reduces the translational energy barrier. Confined fluids undergo a reduction in diffusivity despite similar reduction in the well depth of fluid-fluid and fluid-solid interactions.

To investigate this contrasting behavior, we examine the effective potential energy curve for the solid-fluid and fluid-fluid interactions. In Fig. 3, we have plotted the classical and quantum fluid-solid interactions at 50 K. The classical solid-fluid interaction is temperature independent, and also will be the same for both H_2 and D_2. However, for the quantum fluid, it depends on the mass and temperature as evident from (1), and H_2 displays a stronger effect compared to D_2. Figure 3 shows several differences between the classical and quantum curves, which can affect the diffusivities. In addition to the decrease in well depth, there is an increase in the effective size parameter, estimated as the separation at which the potential becomes zero. Moreover the hardness of the solid-fluid interaction also increases, as is evident from the slope of the potential curve in the repulsive regime, whose magnitude increases from 1623 K Å^{-1} in the classical case to 2153 K Å^{-1} for the quantum fluid. All these effects modify the diffusivity in different ways, however the dominant effect appears to be the steric hindrance caused by the increase in effective size parameter. The increase in the size parameter for solid-fluid and fluid interactions for both H_2 and D_2 is shown as the inset in Fig. 3. As indicated earlier, the diffusion controlling window dimensions for Rho I is 0.543 nm, so that the classical fluids of H_2 and D_2 can pass through without much hindrance. As the effective size parameter increases on decreasing the temperature, H_2 and D_2 face serious hindrance in going from one cage to another through this bottleneck, and this explains the reduction in diffusivity when we include the quantum corrections to the potential. This hindrance, as a result of increase in the size parameter, is greater for H_2 compared to D_2, as seen in the inset of Fig. 3, because of its lower mass.

One of the consequences of the above result is that the extent of drop in the diffusivity of hydrogen is more compared to that of D_2, which leads to D_2 diffusing faster than H_2 below 150 K as shown in Fig. 2. This is also consistent with the observation of effective size increase due to quantum effects. The heavier D_2 has a smaller effective size compared to the lighter H_2 due to the larger quantum effect on the latter, and thereby faces less hindrance in passing through the bottleneck. This leads to a reversal of kinetic selectivity for D_2 and the kinetic selectivity increases with decreasing temperature.

6.2 Corrected potential parameters

In the above simulations we used the Buch parameters to model the H_2-H_2 interaction (Buch 1994). However, to confirm the above unexpected behavior, subsequently we carried out GCMC simulations to verify if these parameters re-

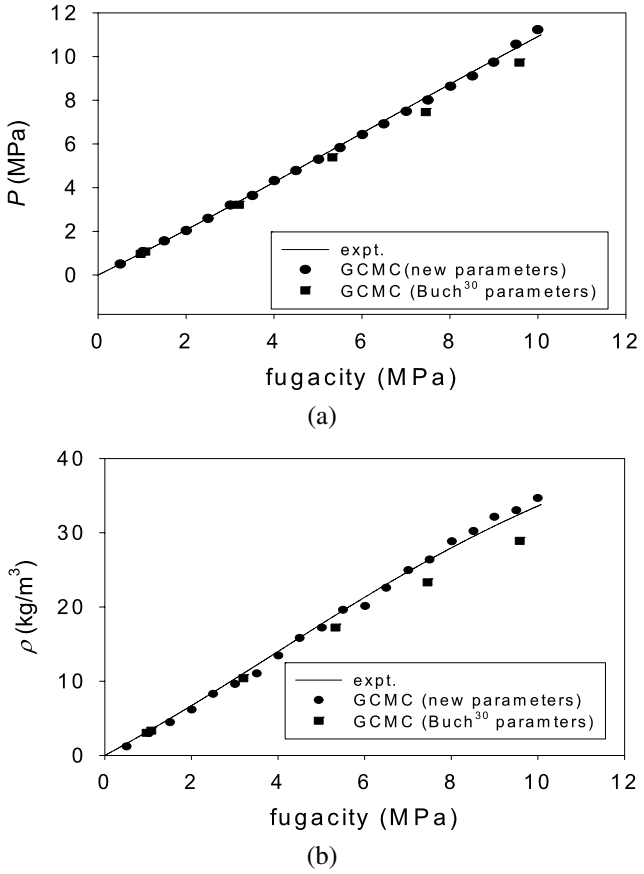

Fig. 4 Pressure and density of bulk H_2 at different fugacities. The *solid line* corresponds to the experimental results and the *symbols* to GCMC simulations

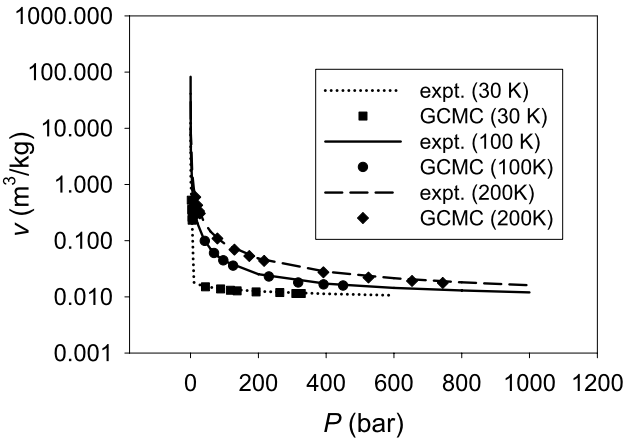

Fig. 5 Specific volume of bulk H_2 versus pressure at different temperatures. The *lines* correspond to experimental values, and the *symbols* to GCMC simulations using the newly obtained potential parameters

produce bulk data when quantum effects are included explicitly. The results are shown in Figs. 4 and 5 along with the experimental data (Younglove 1982; Perry and Green 1998). The line corresponds to the experimental data and the symbols to the results obtained from GCMC simulations using Buch parameters. The state points obtained from the simulations differ from that of experimental data as seen in Fig. 4. To improve these parameters, we performed several GCMC simulations of bulk hydrogen at several state points while using different parameters. The best fitted parameters from these simulations are $\sigma_{H2\text{-}H2} = 0.2782$ nm and $\varepsilon_{H2\text{-}H2} = 38.7$ K. The state points obtained using these parameters are also shown in Figs. 4 and 5. The variations of bulk pressure and density with fugacity at 77 K are shown in Fig. 4 and are in excellent agreement with experimental data (Younglove 1982). We also compared the variation of specific volume with pressure at different temperatures where experimental data is available (Perry and Green 1998), as shown in Fig. 5, which supports the validity of new parameters. The lower value for $\sigma_{H2\text{-}H2}$ and higher value of $\varepsilon_{H2\text{-}H2}/k_BT$ compared to the corresponding Buch parameters are understandable as quantum effects tend to increase the length parameter and decrease the well depth.

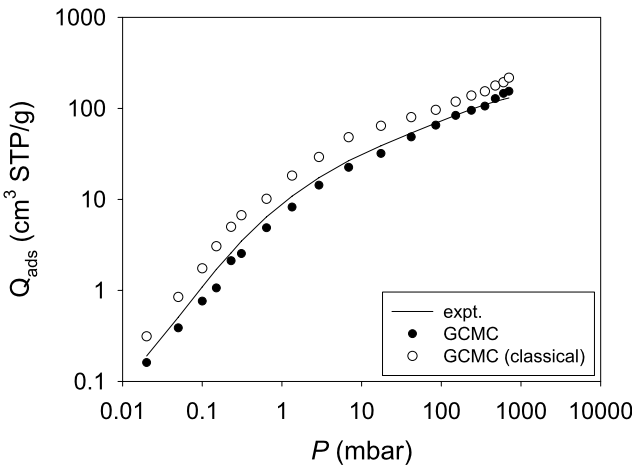

Fig. 6 Hydrogen adsorption isotherm in zeolite Rho II at 80 K. The *solid line* is the experimentally obtained isotherm and the *closed symbols* are from GCMC simulations. *Open symbols* represent the adsorption isotherm obtained from GCMC simulations when quantum corrections are neglected

6.3 Adsorption isotherm

The experimentally obtained adsorption isotherm is used to obtain the solid-fluid interaction parameters. In these studies we used Rho II as the host material, as discussed previously. The best fit obtained from GCMC simulations has been plotted in Fig. 6 along with the experimental isotherm. The potential parameters thus obtained are given in Table 2 and are very similar to the values reported in the literature.

6.4 QENS and MD simulations on Rho II

At the lowest wave vector transfer value of 0.28 $Å^{-1}$, used in our QENS studies, the length scale probed is 22 Å, so that

Table 2 The fitted parameters for fluid-fluid and solid-solid interactions

	σ (nm)	ε/k_B (K)
H_2-H_2	0.2782	38.7
O-O	0.2644	165.02
D-D	0.2762	9.1954
Cs-Cs	0.4959	336.639

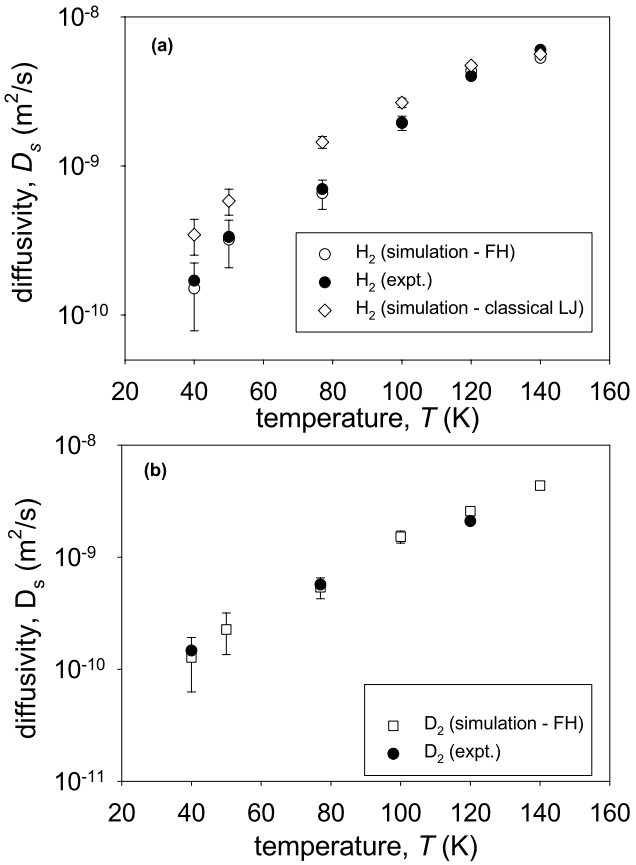

Fig. 7 (**a**) Variation of diffusivity of H_2 (*circles*) in zeolite Rho II with temperatures at a density of 1.4 molecules per unit cell. The MD simulation results for H_2 using the classical L-J potential are also shown (*diamonds*). (**b**) Diffusivity variation of D_2 (*squares*) in zeolite Rho II. In all cases, the *closed symbols* correspond to experimental results and *open symbols* to equilibrium MD simulations

the long range motion corresponding to the cage-to-cage migration can be followed. The spectra were first fitted individually with a Lorentzian function, corresponding to the diffusive motion, convoluted with the instrumental resolution. The spectra were then fitted simultaneously using a jump diffusion model, to extract a diffusion coefficient.

Using the newly obtained parameters, we have carried out canonical ensemble molecular dynamics simulations to model the dynamics of H_2 and D_2 in Rho II. The results obtained from simulations have been compared with those from QENS experiments. The temperature variations of the self diffusivities of H_2 and D_2 at a density of 1.4 molecules

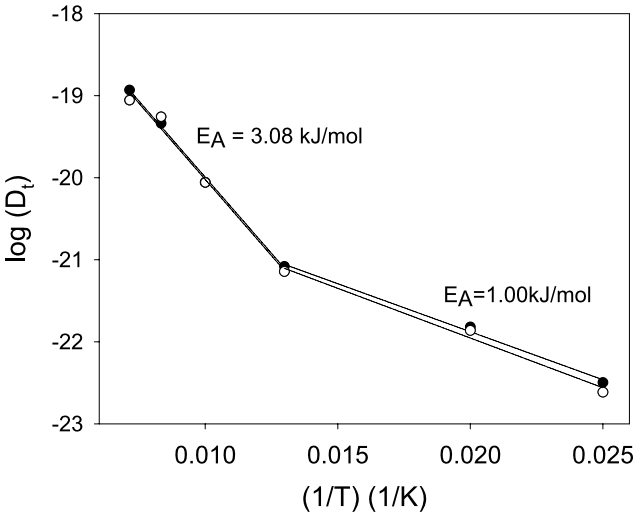

Fig. 8 Natural logarithm of the diffusivity of H_2 against inverse temperature. Here the *closed symbols* are experimental values and *open symbols* from simulation results. The slope changes at 80 K

per unit cell have been plotted in Fig. 7. The closed symbols correspond to QENS results and open symbols to MD simulations. The results are in excellent agreement with each other. Also shown in the figure are the diffusivity values for H_2 in Rho II based on the classical LJ potential, without incorporating the quantum corrections. These classical values are in good agreement with experimental values at high temperatures, while they deviate markedly below 100 K, where the quantum effects are substantial. In this temperature regime, the results obtained using the quantum potential matches closely with the experimental data. These results confirm the importance of quantum effects below 100 K. Here, we do not observe the reversal in kinetic selectivity, seen in our prior simulations on Rho I. As stated before, the zeolite structure we used in this investigation, Rho II, has a larger window dimension than the Rho I material used in the prior simulations. Thus the effective increase in the diameter of H_2 due to quantum effects is not sufficient enough to localize the molecules and block their cage-to-cage migration in Rho II.

Figure 8 depicts the variation in diffusivity with temperature, plotted in Arrhenius coordinates. The closed symbols correspond to experimental data, open symbols to simulation results and the lines are linear fit to the data. From the figure, it is evident that a linear fit in the whole temperature range is not possible, and there is a distinct change in the slope at 80 K. The activation energy changes from 3.0865 kJ/mol above 80 K, to 0.9729 kJ/mol below this temperature for the experimental data. The corresponding values obtained from simulations are 3.0898 kJ/mol and 1.0072 kJ/mol, in substantial agreement with the data.

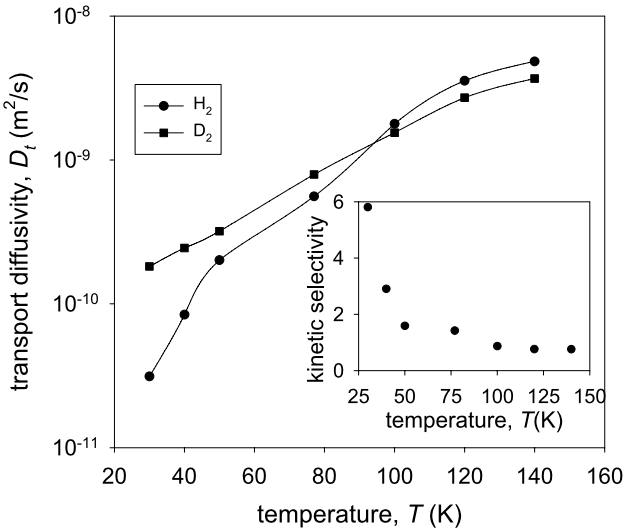

Fig. 9 Temperature variation of the transport diffusivity of H_2 and D_2 in zeolite Rho I. D_2 begins to diffuse faster in this structure around 77 K. The kinetic selectivity of D_2 over H_2 at various temperatures is shown in the *inset*

6.5 MD simulations of H_2 isotopes in Rho I using corrected potential parameters

Using the corrected interaction parameters, discussed earlier, we performed further molecular dynamics simulations of H_2 and D_2 in Rho I to determine the transport diffusivities of hydrogen isotopes. Here, the density of the sorbates was one molecule per the alpha cage of the zeolite Rho, and at this low density, the self-and transport diffusivities are essentially equivalent. However, the transport diffusivity is more appropriate for selectivity and flux calculations and is the quantity considered here. Figure 9 depicts the results. At high temperatures, we observe that H_2 diffuses faster than D_2. However, as the temperature decreases, the ratio between the diffusivity of D_2 to that of H_2 increases, and at approximately 94 K, D_2 begins to diffuse faster than H_2. Around this temperature, H_2 molecules feel the steric hindrance for the cage-to-cage migration, and its diffusivity starts decreasing at a rapid rate, while the deuterium can still pass through the window from one cage to another without much difficulty. Upon decreasing the temperature further, the kinetic selectivity of D_2 increases, and at 30 K, it reaches a value of 5.81. The kinetic selectivity at different temperatures is shown as the inset in Fig. 9. This reversal of kinetic selectivity due to quantum effects, first reported by us in an earlier paper, is supported by the recent experimental work of Zhao et al. (Zhao et al. 2006). These authors report the experimental verification of this kinetic isotope effect for H_2 and D_2 in porous carbon molecular sieves with micropore dimension of 0.546 and 0.566 nm, similar to the smaller window (0.543 nm) zeolite Rho, wherein H_2 shows a slower adsorption/desorption kinetics than D_2 at 77 K. Based on

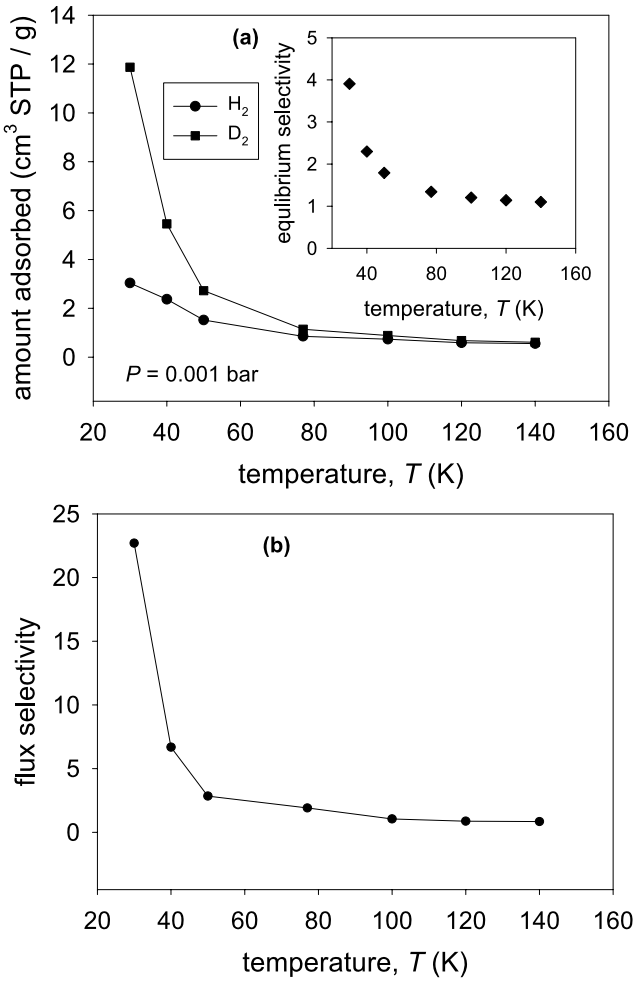

Fig. 10 (**a**) Adsorption isobars of hydrogen and deuterium in zeolite Rho I plotted against temperature. The equilibrium selectivity is shown in the *inset*. (**b**) Temperature variation of flux selectivity of deuterium over hydrogen in zeolite Rho I at low pressure

Fig. 9, we anticipate that the crossover of the diffusivities occurs at about 94 K, so that the faster diffusion of D_2 at 77 K, observed by Zhao et al., is expected given their similar pore size (Zhao et al. 2006).

These investigations point toward the importance of the pore dimension in achieving the reverse kinetic selectivity. We do not observe the reversal of kinetic selectivity in the zeolite Rho II studied here, where the window diameter is 0.596 nm, while we do predict quantum mediated reverse kinetic selectivity for D_2 for the Rho I where the window diameter is 0.543 nm. A difference of 0.05 nm in the pore dimensions results in vastly different dynamic behavior. This shows that the reverse kinetic selectivity is highly sensitive to the pore dimensions and highlights the need to choose the host material judiciously for practical applications.

We have also carried out GCMC simulations of adsorption of hydrogen and deuterium in the structure of zeolite Rho I, to calculate the equilibrium selectivity. The low pres-

sure isobar at different temperatures is plotted in Fig. 10. From the figure, it is evident that heavier deuterium is adsorbed more strongly than lighter hydrogen in the temperature range studied. Moreover, the difference in the amount adsorbed increases with a decrease in temperature. The equilibrium selectivity of deuterium over hydrogen at these temperatures is plotted as the inset in Fig. 10a. The equilibrium selectivity increases as the temperature decreases and is 3.9 at 30 K. These observations are in agreement with earlier investigations of the equilibrium adsorption of hydrogen isotopes in nanopores. The equilibrium and kinetic selectivities obtained here suggest feasibility of zeolite Rho supported membrane separation of hydrogen isotopes. In Fig. 10b, we have plotted the variation of flux selectivity (product of equilibrium and kinetic selectivity) with temperature. At high temperatures, the flux selectivity is rather low; however, at low temperatures, it increases and reaches a value of 22.66 at 30 K. These results confirm the feasibility of separation of H_2 isotopes using microporous materials, and also point towards the narrow regime in pore dimensions where quantum mediated kinetic molecular sieving can be achieved.

7 Conclusions

To conclude, we have carried out atomistic molecular simulations incorporating low temperature quantum effects following the Feynman-Hibbs variational approach and the results are compared with that of QENS experiments. The simulation results are in excellent agreement with experimental results. Based on fits to bulk data and equilibrium adsorption data, we have suggested a new set of potential parameters for H_2-H_2 and H_2-solid interactions, for use with the Feynman-Hibbs variational approach used for incorporating quantum corrections. At low temperatures and narrow pore dimensions, a quantum mediated reverse kinetic molecular sieving can be observed, whereby hydrogen diffuses slower than deuterium. This reverse kinetic molecular sieving is highly sensitive to changes in pore dimensions. The results of these investigations suggest possibility of separation of hydrogen isotopes based on a supported zeolite Rho membrane.

References

Allen, M.P., Tildesley, T.J.: Computer Simulation of Liquids. Oxford University Press, New York (1987)

Beenaker, J.J.M., Borman, V.D., Krylov, S.Y.: Molecular-transport in subnanometer pores-zero point energy, reduced dimensionality and quantum sieving. Chem. Phys. Lett. **232**, 379–382 (1995)

Buch, V.: Path integral simulations of mixed para-d2 and ortho-d2 clusters—the orientational effects. J. Chem. Phys. **100**, 7610–7629 (1994)

Challa, S.R., Sholl, D.S., Johnson, J.K.: Light isotope separation in carbon nanotubes through quantum molecular sieving. Phys. Rev. B **63**, 245419 (2001)

Evans, D., Morris, G.P.: Statistical Mechanics of Nonequilibrium Liquids. Academic, London (1990)

Feynman, R.P., Hibbs, A.R.: Quantum Mechanics and Path Integrals. McGraw-Hill, New York (1965)

Fisher, R.X., Baur, W.H., Shannon, R.D., Staley, R.H., Abrams, L., Vega, A.J., Jorgenson, J.D.: Neutron powder diffraction study and characterization of zeolite D-Rho shallow bed calcined at 773 K. Acta Crystallogr. B **44**, 321–334 (1988)

Guillot, B., Guissani, Y.: Quantum effects in simulated water by the Feynman-Hibbs approach. J. Chem. Phys. **108**, 10162–10174 (1998)

Jobic, H., Karger, J., Bee, M.: Simultaneous measurement of self- and transport diffusivities in zeolites. Phys. Rev. Lett. **82**, 4260–4263 (1999)

Karger, J., Ruthven, D.M.: Diffusion in Zeolites and other Microporous Solids. Wiley-Interscience, New York (1992)

Kiselev, A.V., Du, P.Q.: Molecular statistical calculation of the thermodynamic adsorption characteristics of zeolites using the atom-atom approximation. Part 2. Adsorption of nonpolar and polar inorganic molecules by zeolites of type X and Y. J. Chem. Soc. Faraday Trans. **77**, 1–15 (1981)

Kumar, A.V.A., Bhatia, S.K.: Quantum effect induced reverse kinetic molecular sieving in microporous materials. Phys. Rev. Lett. **95**, 245901 (2005)

Kumar, A.V.A., Jobic, H., Bhatia, S.K.: Quantum effects on adsorption and diffusion of hydrogen and deuterium in microporous materials. J. Phys. Chem. B. **110**, 16666–16671 (2006)

Parise, J.B., Abrams, L., Gier, T.E., Corbin, D.R., Jorgenson, J.D., Prince, E.: Flexibility of the framework of zeolite Rho. Structural variation from 11 to 573 K. A study using neutron powder diffraction data. J. Phys. Chem. **88**, 2303–2307 (1984)

Perry, R.H., Green, D.W. (eds.): Perry's Chemical Engineering Handbook, 7th edn. McGraw-Hill, New York (1998)

Wang, Q.Y., Challa, S.R., Sholl, D.S., Johnson, J.K.: Quantum sieving in carbon nanotubes and zeolites. Phys. Rev. Lett. **82**, 956–959 (1999)

Yang, R.T.: Adsorbents: Fundamentals and Applications. Wiley-Interscience, New York (2003)

Younglove, B.A.: J. Phys. Chem. Ref. Data **11**(Suppl. 1), 1–349 (1982)

Zhao, X., Villar-Rodil, S., Fletcher, A.J., Thomas, K.M.: Kinetic isotope effect for H2 and D2 quantum molecular sieving in adsorption/desorption on porous carbon materials. J. Phys. Chem. B. **110**, 9947–9955 (2006)